nature medicine

A shear gradient–dependent platelet aggregation mechanism drives thrombus formation

Warwick S Nesbitt[1,5], Erik Westein[1,5], Francisco Javier Tovar-Lopez[2], Elham Tolouei[3], Arnan Mitchell[2], Jia Fu[1], Josie Carberry[3], Andreas Fouras[4] & Shaun P Jackson[1]

Platelet aggregation at sites of vascular injury is essential for hemostasis and arterial thrombosis. It has long been assumed that platelet aggregation and thrombus growth are initiated by soluble agonists generated at sites of vascular injury. By using high-resolution intravital imaging techniques and hydrodynamic analyses, we show that platelet aggregation is primarily driven by changes in blood flow parameters (rheology), with soluble agonists having a secondary role, stabilizing formed aggregates. We find that in response to vascular injury, thrombi initially develop through the progressive stabilization of discoid platelet aggregates. Analysis of blood flow dynamics revealed that discoid platelets preferentially adhere in low-shear zones at the downstream face of forming thrombi, with stabilization of aggregates dependent on the dynamic restructuring of membrane tethers. These findings provide insight into the prothrombotic effects of disturbed blood flow parameters and suggest a fundamental reinterpretation of the mechanisms driving platelet aggregation and thrombus growth.

Platelet aggregation at sites of vascular injury is central to the arrest of bleeding and for subsequent vascular repair; however, an exaggerated platelet aggregation response at sites of atherosclerotic plaque rupture can lead to the development of vascular occlusive thrombi, precipitating diseases such as the acute coronary syndromes and ischemic stroke[1–3]. The key variables regulating thrombosis have been known for more than 150 years and include changes in the vessel wall, alterations in the thrombogenic potential of blood and changes in blood flow parameters (hemodynamics)[4]. Although the former two variables have a well defined role in arterial thrombosis, the mechanism by which alterations in blood flow affects the thrombotic process remains ill defined.

Platelet aggregation under the influence of blood flow is dependent on the adhesive function of both the platelet glycoprotein (GP) Ib-V-IX receptor complex and integrin $\alpha_{IIb}\beta_3$ (also known as GP IIb-IIIa), wherein GPIb initiates reversible platelet recruitment, particularly at elevated shear rates, and integrin $\alpha_{IIb}\beta_3$ stabilizes forming aggregates[5–12]. A primary step regulating the transition from reversible to stable adhesion is activation of integrin $\alpha_{IIb}\beta_3$, a process dependent on the generation of the soluble agonists adenosine diphosphate (ADP), thromboxane A_2 (TXA_2) and thrombin[2,5,6]. Soluble agonists stimulate a host of biochemical and functional responses, including cytosolic calcium flux, platelet shape change and granule release, that coincide with the rapid development of platelet aggregates[13]. However, the recent demonstration that platelets can form aggregates *in vivo* without a detectable increase in cytosolic calcium[14,15], without undergoing shape change[15,16] and without substantial α-granule secretion in the early phases of thrombus development[17] has raised the possibility that additional mechanisms may be involved[16,18].

One such mechanism may involve local changes in blood flow. Recent studies have identified that, in the range of physiological blood shear (strain) rates (1,000–10,000 s^{-1}), small, transient discoid platelet aggregates can form through the development of membrane tethers[16], whereas at pathological shear rates (>10,000 s^{-1}) large rolling aggregates can develop independently of integrin $\alpha_{IIb}\beta_3$ and platelet activation[18]. How important these rheologically driven aggregation mechanisms are, relative to soluble agonist-generated aggregates, in promoting thrombus development *in vivo* remains unclear. In this study we show that rapid changes in blood flow (shear microgradients) represent a general feature of thrombus development, inducing stabilized aggregation of discoid platelets. This shear-regulated platelet aggregation mechanism involves a unique biomechanical sensing mechanism linked to the physical restructuring of membrane tethers. Our findings suggest that mechanosensory platelet activation mechanisms have a major role in driving platelet aggregation and thrombus growth *in vivo*.

RESULTS

Shear microgradients promote discoid platelet aggregation

It has long been recognized that platelet aggregation preferentially occurs at regions of flow disturbance after vascular injury[19,20]. To investigate the effects of rheological disturbance on platelet aggregation dynamics *in vivo*, we employed intravital imaging to visualize the platelet aggregation process in mesenteric arterioles of mice. We

[1]The Australian Centre for Blood Diseases, Monash University, Alfred Medical Research and Educational Precinct, Melbourne, Victoria, Australia. [2]Microelectronics and Materials Technology Centre, School of Electrical and Computer Engineering, RMIT University, Melbourne, Victoria, Australia. [3]Department of Mechanical Engineering and [4]Division of Biological Engineering, Monash University, Clayton, Victoria, Australia. [5]These authors contributed equally to this work. Correspondence should be addressed to W.S.N. (warwick.nesbitt@med.monash.edu.au) or S.P.J. (shaun.jackson@med.monash.edu.au).

Received 17 October 2008; accepted 27 March 2009; published online 24 May 2009; doi:10.1038/nm.1955

initiated platelet adhesion and aggregation by mild crush injury of the vessel wall and monitored platelet thrombus formation via differential interference contrast (DIC) microscopy (**Fig. 1a**). We altered blood flow by compressing the vessel side wall at the site of injury, using a blunted microinjection needle to progressively stenose the vessel lumen (**Fig. 1a**). Localized stenosis markedly accelerated the rate and extent of platelet aggregation (**Fig. 1a**; 16.39 s), particularly when stenosis was greater than ~90%. Notably, thrombi appeared to be composed of loosely packed platelets, suggesting that minimal platelet activation had occurred (data not shown). Thrombus formation was dynamic with cycles of aggregation and disaggregation corresponding to serial increases and decreases in stenosis, with removal of the microinjector needle leading to disaggregation of the platelet mass (**Fig. 1a**; 24.13 s). Stenosis in the absence of vessel injury did not result in platelet aggregation, indicating that flow changes *per se* were insufficient to induce platelet aggregation (data not shown).

To gain insight into the relationship between localized flow changes and platelet aggregation we performed computational fluid dynamic (CFD) modeling of the stenosed vessel geometry. Temporal analysis of thrombus formation after vessel stenosis revealed that initial platelet recruitment occurred specifically at the stenosis apex (**Fig. 1a**), with the subsequent formation of discoid platelet aggregates occurring in the downstream expansion zone (**Fig. 1a**). We observed platelet aggregation throughout the expansion zone, but aggregation rapidly ceased at the downstream margin of this zone (**Fig. 1a**), suggesting that the stenosis had a spatially restricted effect on thrombus growth. CFD modeling of the *in vivo* vessel geometry predicted blood shear rates (γ) $\geq$ 20,000 s^{-1} at the stenosis apex that rapidly transitioned to $\leq$862 s^{-1} within the post-stenosis expansion zone (**Fig. 1b**), suggesting that a zone of shear acceleration followed by a zone of decelerating shear (shear microgradient) may be a requirement for the development of discoid platelet aggregates (**Fig. 1b**).

To examine the specific effect of localized shear microgradients on platelet aggregation dynamics, independent of potential non-hemodynamic effects on the vessel wall, we designed model microchannels incorporating a fixed stenosis. These geometries were characterized by a backward-facing step of defined 90% stenosis immediately followed by an expansion zone (**Fig. 1c**). This geometry generates a localized region of rapid flow acceleration followed by a zone of flow deceleration (**Supplementary Fig. 1a** online).

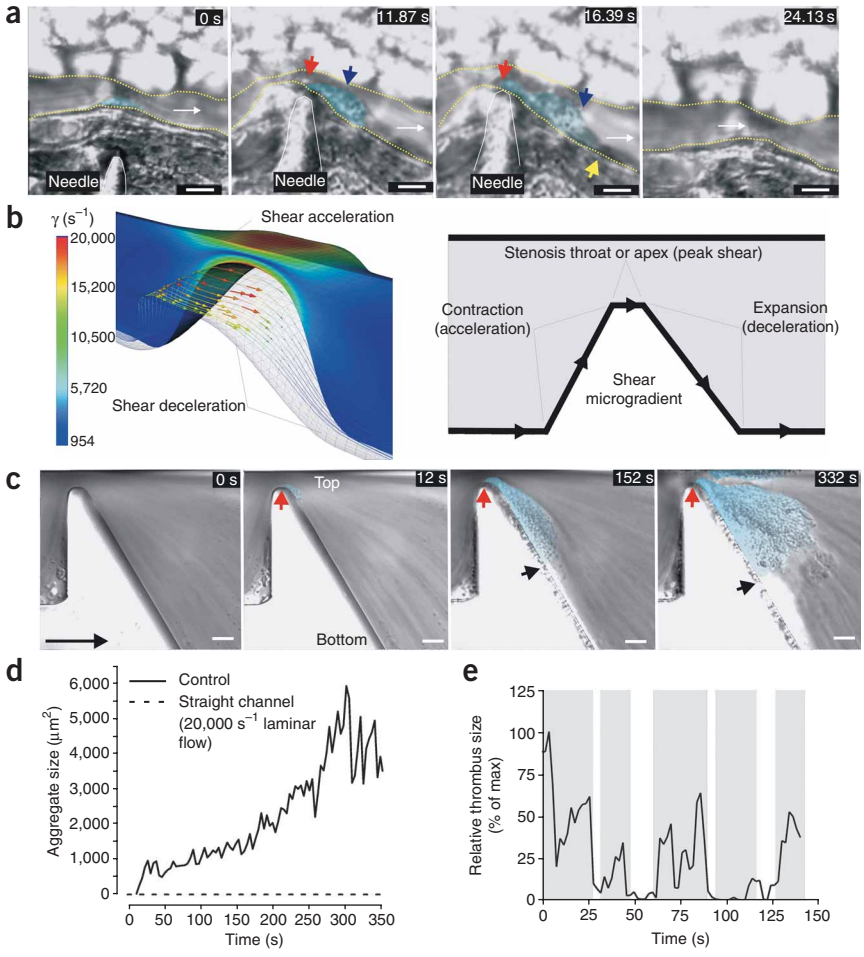

Figure 1 Shear microgradients promote platelet aggregate formation *in vivo*. (**a**) DIC images demonstrating the effect of localized vascular stenosis on platelet aggregation after localized crush injury of a mouse mesenteric arteriole ($n = 3$ experiments). Small platelet aggregates are present at $t = 0$ s (cyan shading). After stenosis (11.87 s), a marked increase in platelet aggregation was observed (blue arrow), which specifically developed downstream from the site of vascular injury (red arrow). Aggregate growth ceased at the downstream stenosis margin (yellow arrow; 16.39 s) where the vessel returned to its native geometry. Subsequent removal of the microneedle led to the rapid embolization of the platelet aggregate (24.13 s). Scale bars, 10 μm. (**b**) CFD simulation of blood flow dynamics after localized vessel wall compression (left) and schema illustrating the three principal components defining a shear microgradient or stenosis (right). The contraction demarcates the region of shear acceleration. The throat or apex demarcates the stenotic region at which peak shear is experienced. The expansion demarcates the region of shear deceleration. The CFD simulation demonstrates that for a predicted input shear of 1,800 s^{-1} (immediately upstream from the stenosis), flow accelerates into the stenosis throat, reaching a maximum shear of $\geq$20,000 s^{-1} at the apex. This elevated shear rapidly decelerates in the downstream expansion zone of the geometry, transitioning from 20,000 to 862 s^{-1} at the downstream margin of the expansion (yellow arrows). (**c**) DIC image sequence of blood perfusion through a microchannel comprising a side-wall geometry designed to induce a sharp phase of accelerating shear from 1,800 s^{-1} coupled to an immediate shear deceleration approaching 200 s^{-1}. Red arrow indicates the point of initial aggregation ($t = 12$ s) and black arrow indicates the limit of thrombus growth in the expansion zone (representative of $n = 3$ experiments). (**d**) Representative aggregation traces showing the response of whole-blood perfusion through the microchannel in **c**. Control, hirudin-anticoagulated whole-blood perfusion at an input (prestenosis) shear rate of 1,800 s^{-1} (representative of $n = 3$ experiments); straight channel, hirudin-anticoagulated whole-blood perfusion through a 100-μm straight (control) microchannel at a bulk shear rate of 20,000 s^{-1} (representative of $n = 3$ experiments). (**e**) Relative thrombus size (% of maximum size) in wild-type mouse arterioles as a function of applied downstream vessel compression (gray bars represent the periods of flow deceleration due to vessel compression) showing a direct correlation between reduced bulk flow rate and increased thrombus size (DIC two-dimensional surface area in μm^2; representative of $n = 4$ experiments).

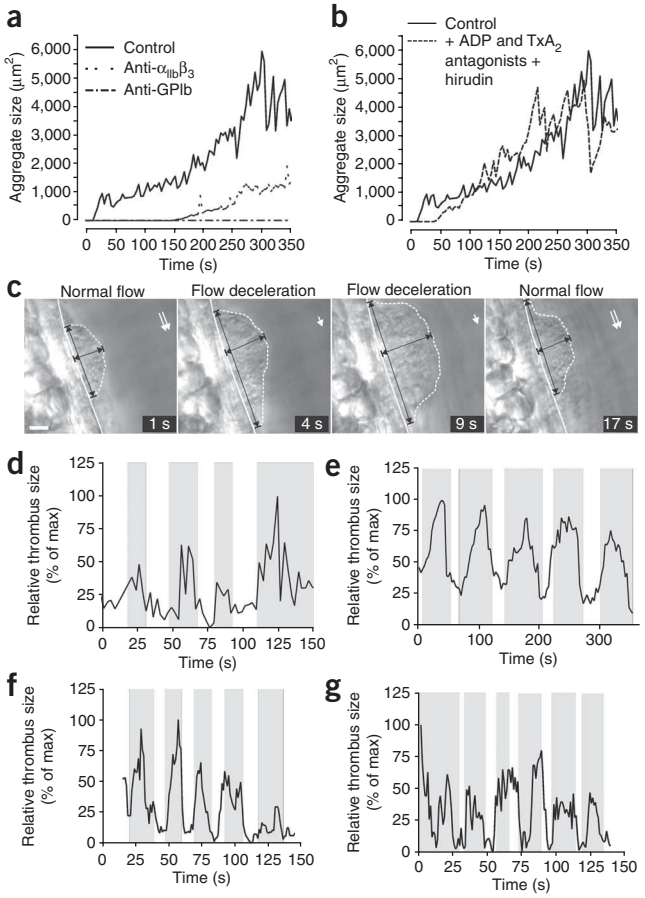

Figure 2 Platelet aggregation induced shear microgradients occurs independently of ADP, TXA_2 and thrombin. (**a**) Aggregation traces showing the response of whole-blood perfusion through the microchannel depicted in **Figure 1c**. Control, hirudin-anticoagulated whole-blood perfusion at an input (prestenosis) shear rate of 1,800 s^{-1} (representative of $n = 3$ experiments); anti-$\alpha_{IIb}\beta_3$, hirudin-anticoagulated whole blood treated for 10 min with 30 μg ml^{-1} c7E3 Fab before blood perfusion (representative of $n = 3$ experiments); anti-GPIb, hirudin-anticoagulated whole blood treated for 10 min with 50 μg ml^{-1} of the GPIb blocking IgG ALMA12 (representative of $n = 3$ experiments). (**b**) Microchannel aggregation as in **a**. Control, hirudin-anticoagulated whole-blood perfusion at an input (prestenosis) shear rate of 1,800 s^{-1}; +ADP and TXA_2 antagonists + hirudin, hirudin-anticoagulated whole blood treated for 10 min with MRS2179 (100 μM), 2-MeSAMP (10 μM) and indomethacin (10 μM) (representative of $n = 3$ experiments). (**c**) Representative DIC imaging showing the impact of downstream vessel compression and resultant flow deceleration on platelet aggregate growth at a site of vessel crush injury ($n = 4$ experiments). Dotted marquee highlights the outer perimeter of the developing discoid platelet aggregate. Solid line indicates the vessel wall. Black arrows highlight both relative length and height increase. Scale bar, 10 μm. (**d**–**g**) Relative thrombus size (% of maximum size) in mouse arterioles as a function of applied downstream vessel compression (gray bars represent periods of flow deceleration due to vessel compression) (DIC two-dimensional surface area in μm^2) in wild-type mice (**d**), wild-type mice pretreated orally with 10 mg per kg body weight clopidogrel and 200 mg per kg body weight aspirin (**e**), wild-type mice pretreated with 50 mg per kg body weight hirudin (**f**) or *P2Y1*$^{-/-}$mice pretreated with 50 mg per kg body weight clopidogrel and 200 mg per kg body weight aspirin and 50 mg per kg body weight hirudin (**g**). In **d**–**g**, $n = 4$ experiments in three mice per condition.

Whole-blood perfusion through this microchannel indicated that discoid platelet aggregation was induced specifically by microscale changes in shear (**Fig. 1c**,**d**). As was the case *in vivo*, initial platelet recruitment occurred within the zone of peak shear, whereas large discoid platelet aggregates occurred within the boundaries of the deceleration zone (**Fig. 1c**). Platelet aggregation seemed to be influenced by the magnitude of the shear gradient, as reducing the rate of shear deceleration, by altering the expansion angle, resulted in a marked decrease in platelet aggregate formation (data not shown). Furthermore, in the absence of shear microgradients platelet aggregation did not initiate even under conditions of elevated shear (**Fig. 1d** and **Supplementary Fig. 1b**).

To directly examine the relationship between shear deceleration and discoid platelet aggregation *in vivo*, in the absence of a localized stenosis, we conducted experiments in mouse mesenteric arterioles in which blood flow rates were progressively decelerated by compression of the vessel ~100 μm downstream from the injury site (**Supplementary Fig. 1c**,**d**). Progressive deceleration of blood flow had a marked effect on aggregate growth, amplifying both the rate and the extent of discoid platelet aggregation, such that serial acceleration and deceleration of blood flow correlated directly with serial increases and decreases in discoid platelet aggregation, respectively (**Fig. 1e** and **Supplementary Video 1** online). Taken together, these studies demonstrate a major role for localized shear microgradients, and specifically the shear deceleration phase, in enhancing discoid platelet aggregation.

Platelet adhesion receptors and shear microgradient aggregation

Platelet aggregation under physiological shear conditions requires the cooperative function of two major platelet adhesion receptors, GPIb and integrin $\alpha_{IIb}\beta_3$, with the relative contribution of each receptor dependent on local hemodynamic conditions[5]. To investigate the role of these receptors in promoting shear microgradient–dependent platelet aggregation, we examined the effects of blocking GPIb or integrin $\alpha_{IIb}\beta_3$ function on discoid platelet aggregation in microchannel flow experiments. Inhibition of the ligand binding function of GPIb revealed an absolute requirement for this receptor in initiating platelet recruitment to the peak shear zone in the microchannel (**Fig. 2a**). In contrast, blocking integrin $\alpha_{IIb}\beta_3$ function had no inhibitory effect on initial platelet recruitment to the high-shear zone, but it markedly inhibited platelet aggregation in the downstream deceleration zone (**Fig. 2a**), demonstrating distinct functions for these receptors.

Platelet activation at sites of vascular injury is stimulated by soluble agonists, principally ADP, TXA_2 and thrombin. To investigate the role of these agonists in promoting shear microgradient–dependent platelet aggregation, we determined the effects of blocking TXA_2 generation (with the cyclooxygenase inhibitor indomethacin), ADP (with apyrase, in combination with the $P2Y_1$ and $P2Y_{12}$ inhibitors MRS2179 and 2-MeSAMP, respectively) and thrombin (with hirudin) on discoid platelet aggregation in microchannel flow experiments. Notably, eliminating the platelet-activating effects of ADP, TXA_2 and thrombin had no effect on platelet aggregation dynamics induced by local shear microgradients (**Fig. 2b** and **Supplementary Video 2** online). Even in the complete absence of soluble agonists, stabilized discoid platelet aggregates were able to persist for the full duration of blood perfusion (up to 10 min); however, they remained reversible and rapidly disaggregated after cessation of flow (data not shown). These studies show that shear microgradients can induce sustained aggregation of discoid platelets independently of soluble agonists.

To investigate whether platelet aggregation induced by shear deceleration *in vivo* is dependent on soluble agonists, we examined the effects of blocking TXA_2 generation (with aspirin), ADP (with clopidogrel and with the use of *P2Y1*$^{-/-}$ mice which lack the $P2Y_1$ ADP receptor) and thrombin (with hirudin) on discoid platelet

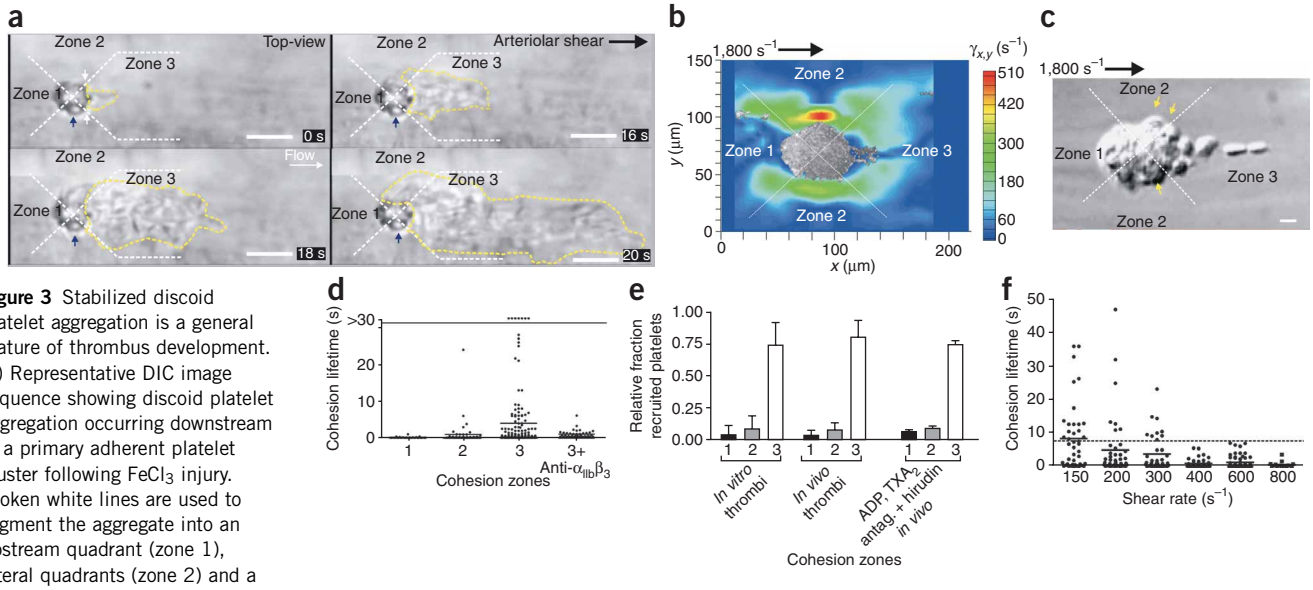

Figure 3 Stabilized discoid platelet aggregation is a general feature of thrombus development. (**a**) Representative DIC image sequence showing discoid platelet aggregation occurring downstream of a primary adherent platelet cluster following $FeCl_3$ injury. Broken white lines are used to segment the aggregate into an upstream quadrant (zone 1), lateral quadrants (zone 2) and a downstream quadrant (zone 3). Blue arrow indicates lesion caused by $FeCl_3$ treatment, white arrows the points at which initial platelet recruitment was observed and broken yellow line the outer margin of the discoid platelet aggregate. Scale bars, 5 μm. (**b**) *In vitro* micro-PIV analysis of planar shear rates ($\gamma_{x,y}$) within 2 μm of the microchannel floor (bulk $\gamma = 1{,}800\ s^{-1}$). The thrombus is segmented as in **a**. Representative of $n = 3$ experiments. (**c**) Representative DIC image showing discoid platelet tethering to an *in vitro* thrombus at an applied shear rate of $1{,}800\ s^{-1}$. Note that initial platelet recruitment occurs at the zone 2–3 boundary (yellow arrows) and the predominance of stabilized discoid platelet tethering in zone 3. Scale bar, 2 μm. (**d**) Discoid platelet cohesion lifetimes in zones 1, 2 and 3 *in vitro* ($n = 24$ experiments). Horizontal bar represents 30-s cutoff. Anti-$\alpha_{IIb}\beta_3$, platelets treated for 10 min with 30 μg ml^{-1} c7E3 Fab before blood perfusion. (**e**) Proportion of discoid platelets tethering within zones 1, 2 and 3 of developing mouse thrombi *in vitro* and *in vivo*. *In vitro* thrombi, cohesion frequency at the surface of *in vitro* thrombi ($n = 24$ experiments); *in vivo* thrombi, cohesion frequency at the surface of *in vivo* thrombi in C57BL/6 wild-type mice ($n = 14$); ADP, TXA_2 antagon. + hirudin *in vivo*, cohesion frequency at the surface of *in vivo* thrombi in *P2Y1*$^{-/-}$ mice administered with 200 mg per kg body weight aspirin, 50 mg per kg body weight clopidogrel orally + intravenous hirudin (50 mg per kg body weight) ($n = 14$). Values are as mean ± s.e.m. (**f**) Discoid platelet cohesion lifetimes at the surface of preformed platelet monolayers as a function of applied bulk shear rate (γ) ($n = 3$). Horizontal bar represents arbitrary 8-s cutoff.

aggregation in mesenteric arterioles as a function of flow deceleration (**Fig. 2c**,**d** and **Supplementary Fig. 1c**,**d**). Pretreatment of mice with combined clopidogrel and aspirin or with hirudin had no inhibitory effect on discoid platelet aggregation induced by shear deceleration (**Fig. 2e**,**f**), such that serial deceleration and acceleration of blood flow induced corresponding increases and decreases in aggregate size, respectively. Similarly, eliminating the platelet-activating effects of ADP, TXA_2 and thrombin altogether by pretreating *P2Y1*$^{-/-}$ mice with high-dose clopidogrel, hirudin and aspirin also failed to inhibit platelet aggregation induced by flow deceleration (**Fig. 2g**). These studies show that flow deceleration can promote discoid platelet aggregation *in vivo*, independently of soluble agonists.

Stabilized discoid aggregates are a general feature of thrombosis

It has previously been shown that discoid platelets form adhesive interactions with the superficial layers of forming thrombi; however, these adhesive interactions are rapidly reversible, leading to persistent platelet detachment from the thrombus surface[16]. To investigate the potential contribution of stabilized discoid platelet aggregation to thrombus development in nonstenosed vessels, we examined thrombus formation in four distinct vascular injury models: mechanical crush injury (**Fig. 1a**), mechanical vessel wall puncture (data not shown), photoactivation of Rose Bengal (4,5,6,7-tetrachloro-2′,4′,5′,7′-tetraiodofluorescein) (**Supplementary Video 3** online) and topical application of $FeCl_3$ (**Fig. 3a**). A key feature in all models was the prominence of stabilized discoid platelet aggregation during thrombus development, constituting >80% of the total thrombus mass within the first 3 min of the period after injury and remaining at >40% of the total thrombus 5–10 min after injury (**Supplementary Video 4** online). Whereas the outer superficial layers of forming thrombi (that experience maximal hemodynamic drag force) consisted of transiently tethering discoid platelets (cohesion lifetimes of 0.33 ± 0.21 s), stabilized discoid platelet aggregates incorporated into deeper layers of the developing thrombus (which are thereby protected from flow) could remain stationary for >5 min (data not shown). As a result, stabilized discoid aggregates were able to propagate into the vessel lumen and had sufficient tensile strength to transiently occlude blood vessels (**Supplementary Video 3**).

Spatiotemporal analysis of thrombus development revealed that stabilized discoid platelet aggregates primarily formed downstream of the site of vascular injury (**Fig. 3a**). These aggregates were dynamic, with phases of aggregate growth and embolization occurring throughout the 10-min period after injury (data not shown). Consolidation of stabilized discoid platelet aggregates always developed from the site of injury and was associated with the loss of discoid morphology and tight packing of aggregated platelets within the thrombus base (**Supplementary Fig. 2** and **Supplementary Video 4** online). This consolidation phase was dependent on soluble agonists, as it was completely eliminated by blocking the combined platelet activating effects of TXA_2, ADP and thrombin (data not shown). These studies show a major role for stabilized discoid platelet aggregation in driving thrombus propagation, particularly downstream of the site of vascular injury, whereas soluble agonists seem to have a secondary role in consolidating formed aggregates.

Hemodynamics spatially regulate platelet aggregation

To gain insight into the contribution of hemodynamic changes in regulating the spatial accumulation of platelets onto the surface of

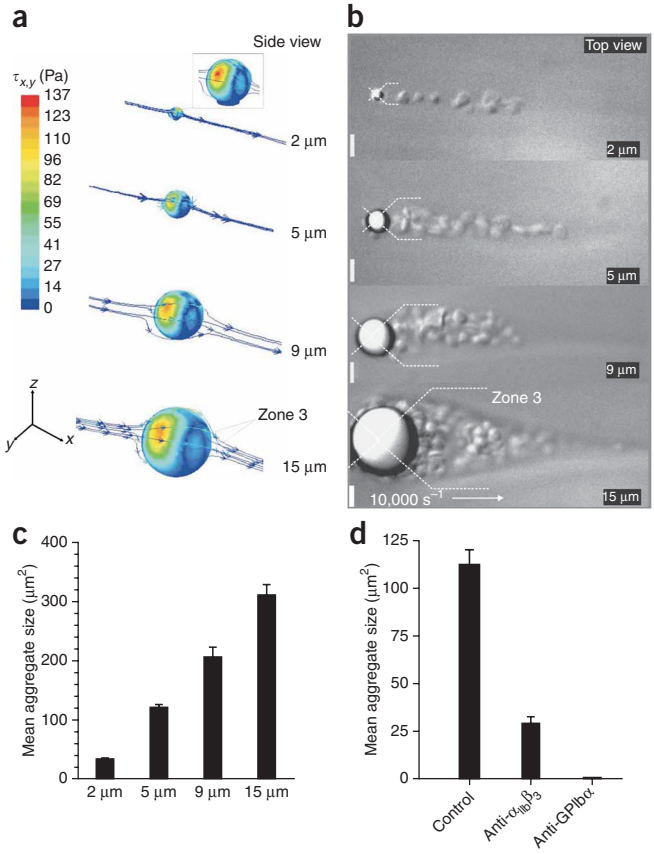

Figure 4 The magnitude and spatial distribution of the shear microgradient directly affects platelet aggregate size. (**a**) CFD simulation of blood planar shear stresses ($\tau_{x,y}$) around microspheres at the surface of 0.2 × 2 mm microcapillaries (bulk shear rate = 10,000 s^{-1}); inset, magnified view of the 2-μm bead case. Note the increase in spatially varying shear stress at the bead sides ($\tau_{x,y}$) as a function of bead diameter and the creation of a low shear zone (zone 3) at the downstream face of the beads, the size of which is directly dependent on bead diameter. Planar shear stress ($\tau_{x,y}$) represents the predicted stress experienced by a free flowing platelet as it approaches within 1 μm (one-half of discoid platelet diameter) of the bead surface. Side view is shown for all beads. (**b**) DIC image frames showing the nature and extent of discoid platelet aggregation at the downstream face of vWF-coated microbeads after whole-blood (pretreated with 100 μM MRS2179, 10 μM 2-MeSAMP and 10 μM indomethacin) perfusion at an applied γ of 10,000 s^{-1} ($n = 5$). Aggregation occurs exclusively at the downstream (zone 3) face of the beads, and aggregates can extend up to seven bead diameters downstream of initial platelet-bead adhesion, with overall aggregate width correlating with bead diameter. Top view is shown for all beads. (**c**) Mean discoid platelet aggregate size (surface area in μm^2 ± s.e.m.) as a function of microbead diameter ($n = 3$). (**d**) Mean (± s.e.m.) discoid platelet aggregate size at the downstream face of 5-μm vWF-coated microbeads at an applied bulk shear rate of 10,000 s^{-1}. Control, hirudin-anticoagulated whole blood; anti-$\alpha_{IIb}\beta_3$, hirudin-anticoagulated whole blood treated for 10 min with 30 μg ml^{-1} c7E3 Fab; anti-GPIb, hirudin-anticoagulated whole blood treated for 10 min with 50 μg ml^{-1} of the GPIb-blocking IgG ALMA12 ($n = 3$).

thrombi, we developed a microscale particle imaging velocimetry (micro-PIV) approach to quantitatively map the planar shear ($\gamma_{x,y}$) environment around thrombi (**Fig. 3b** and **Supplementary Fig. 3** online). Examination of the planar ($\gamma_{x,y}$) shear rates around an *in vitro* thrombus at an applied bulk shear of 1,800 s^{-1} revealed the development of three spatially distinct shear zones at the thrombus surface. At the leading edge of thrombi (zone 1), shear ($\gamma_{x,y}$) was minimal, equivalent to free flow regions elsewhere in the flow channel (**Fig. 3b** and **Supplementary Fig. 3**). However, on the thrombus sides (parallel to the direction of flow; zone 2) marked lateral shear acceleration ($\gamma_{x,y}$ = 240 s^{-1} to >510 s^{-1}) occurred (**Fig. 3b**). At the downstream face of thrombi (zone 3), a distinct low-shear pocket developed ($\gamma_{x,y}$ = 0–120 s^{-1}; **Fig. 3b**). Notably, the spatial distribution of shear remained the same over a broad range of applied flow rates (**Supplementary Fig. 3**). These studies show that thrombi generate spatially discrete shear zones, with shear deceleration becoming prominent at the downstream thrombus face.

Analysis of platelet recruitment to thrombi revealed that initial recruitment typically occurred in the shear acceleration zone on the sides of thrombi (zone 2; **Fig. 3c** and **Supplementary Video 4**). These initial interactions were labile (cohesion lifetimes 0.18 ± 0.11 s), resulting in rapid platelet translocation into the low-shear zone at the downstream face (zone 3) (**Fig. 3d** and **Supplementary Video 5** online). Once in zone 3, these tethered discoid platelets underwent stabilization, resulting in a >50-fold increase in cohesion lifetimes (from 0.18 s to ≥30 s; (**Fig. 3d**)). As a consequence, >75% of stable discoid platelet aggregation occurred within this low-shear pocket (**Fig. 3e**). This proportion did not change with inhibition of soluble agonists (data not shown); however, recruitment to the low-shear zone was eliminated by integrin $\alpha_{IIb}\beta_3$ blockade (**Fig. 3d**). We observed a similar pattern of platelet recruitment for thrombus development *in vivo* (**Fig. 3e** and **Supplementary Videos 4** and **5**). These findings indicate that local shear microgradients generated by developing thrombi, and more specifically decelerating shear at the downstream face of thrombi, directly induce stabilization of discoid platelet aggregates.

To examine the relationship between shear and stabilization of discoid platelet adhesion more directly, we performed platelet perfusion experiments on platelet monolayers over a laminar shear range covering those measured at the surface of thrombi (**Fig. 3f**). These studies showed a direct inverse correlation between shear and adhesion lifetimes of discoid platelets, such that at 800 s^{-1} all discoid platelet adhesive interactions were highly unstable (mean tethering time of <2 s), whereas we observed increased platelet adhesion lifetimes with progressive reductions in shear, similar to those occurring at the downstream face of forming thrombi (**Fig. 3f**). Overall, these studies support a model in which local changes in blood hemodynamics around forming thrombi directly modify the stability of discoid platelet adhesive interactions.

Shear microgradient magnitude determines aggregate size

The demonstration that thrombi promote stabilized discoid platelet aggregation by locally modulating blood flow raised the possibility that the magnitude of locally generated shear microgradients is a major determinant of overall aggregate size. To test this hypothesis directly, we developed a 'bead collision assay', in which we immobilized polystyrene microspheres of varying sizes (2-, 5-, 9- and 15-μm diameter), precoated with purified human von Willebrand factor (vWF), at the surface of glass microcapillaries to induce controlled localized changes in blood flow. CFD analysis of shear stress ($\tau_{x,y}$) distributions at the bead surface predicted a direct correlation between bead size and the spatial distribution of shear gradients, such that the beads create a lateral zone of accelerating shear that is closely coupled to a downstream low shear (≤30.4 Pa) pocket, the size of which is directly dependent on bead diameter (**Fig. 4a** and **Supplementary Fig. 4a**,**b** online). Blood flow around these microspheres led to the rapid development of stable discoid platelet aggregates (independently of soluble agonists), the location and size of which directly correlated with the location and extent of the low-shear zone (**Fig. 4b**,**c**).

Notably, the nature and extent of aggregation was equivalent to that observed during the early stages of thrombus development *in vivo*. Much as our earlier findings had indicated (**Figs. 2a** and **3d**), GPIb was essential for the initiation of platelet aggregation, whereas integrin $\alpha_{IIb}\beta_3$ engagement stabilized discoid platelet aggregates (**Fig. 4d**). These studies show that the magnitude and spatial distribution of shear microgradients directly influences platelet aggregate size.

Tether restructuring mediates shear gradient aggregation

A characteristic feature of high-shear platelet adhesion is the development of filamentous membrane tethers—cylinders of lipid bilayer pulled from the surface of discoid platelets by hemodynamic extensional forces[16,18,21]. Membrane tethers support platelet-matrix and platelet-platelet adhesion; however, these adhesive interactions are typically transient in the absence of platelet stimulation by soluble agonists[16,18,21]. Analysis of platelet adhesion to the surface of *in vitro* thrombi revealed that the majority of discoid platelets stably adhering within the decelerating shear zone (zone 3) of developing thrombi showed adhesive characteristics indicative of membrane tether formation, characterized by free movement or rotation of platelets around a fixed anchor point and extension and recoiling of individual platelets from the thrombus surface (**Fig. 5a,b**, **Supplementary Fig. 5** and **Supplementary Video 5** online). Of note, stabilized discoid platelet tethering in response to shear deceleration was associated with tether restructuring, leading to the development of thickened bulbous membrane tethers (**Fig. 5a,b**, **Supplementary Fig. 5a** and **Supplementary Video 5**). We observed this restructuring event in platelets tethering to thrombi (**Fig. 5a**) and to platelet monolayers (**Fig. 5b** and **Supplementary Fig. 5**). Observation of discoid platelet tethering interactions onto the surface of platelet monolayers indicated that tether restructuring only occurs at or below an applied shear rate of 300 s^{-1}, indicating that tether restructuring represents a shear-sensitive functional response.

To investigate the impact of tether restructuring on the adhesive function of discoid platelets, we correlated tether morphology with platelet adhesive behavior as a function of shear. At shear rates >300 s^{-1}, all discoid platelets formed thin filamentous tethers that were incapable of supporting prolonged platelet-platelet adhesive

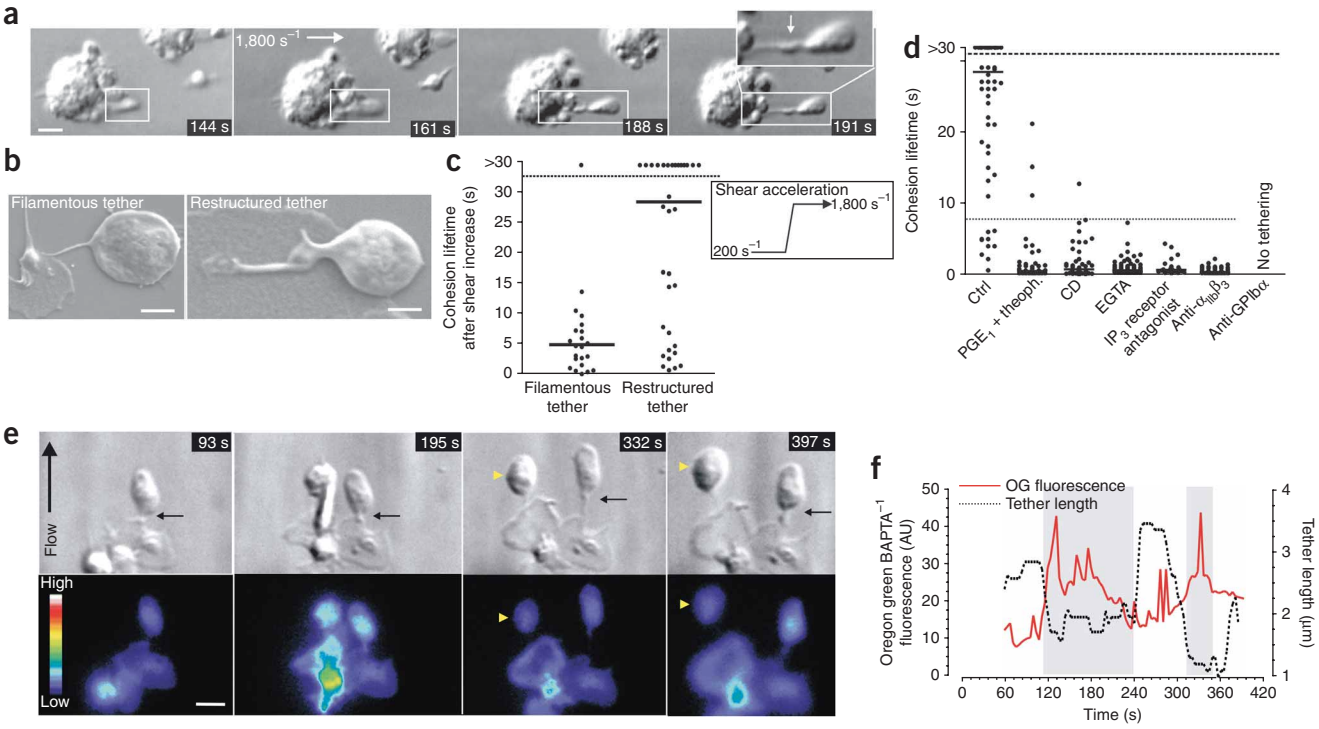

Figure 5 Stabilized discoid platelet aggregation occurs via restructuring of membrane tethers. (**a**) DIC imaging showing dynamic platelet tether behavior at the downstream face of a thrombus, preformed on an immobilized type 1 fibrillar collagen (applied bulk shear rate = 1,800 s^{-1}). Scale bar, 2 μm. The white box highlights the progression of a discoid platelet tether: initial platelet interaction results in the formation of a short tether (144 s) that rapidly thickens (161–188 s) to produce a bulbous membrane structure proximal to the discoid body (white arrow; 191 s). (**b**) Scanning electron micrograph of discoid platelets exhibiting filamentous and restructured membrane tethers during adhesion to the surface of spread platelet monolayers (applied bulk shear rate = 300 s^{-1}). Scale bars, 1 μm. (**c**) Tether cohesion lifetimes as a function of tether morphology and shear acceleration. Discoid platelets were allowed to tether to preadherent platelet monolayers at an applied shear rate of 200 s^{-1} for 2 min followed by shear acceleration to 1,800 s^{-1} (inset). Tethers were visually classified as filamentous or restructured tethers ($n = 3$ experiments). (**d**) Cohesion lifetimes of tethered discoid platelets on the surface of platelet monolayers at an applied shear rate of 300 s^{-1}. Ctrl, control; anti-$\alpha_{IIb}\beta_3$, pretreated with 30 μg ml^{-1} c7E3 Fab; EGTA, 5 mM EGTA; IP_3 receptor antagonist, 50 μM 2-aminoethoxyphenyl borate; CD, 20 μM cytochalasin D; PGE1 + theoph., 2 μg ml^{-1} PGE1 and 10 mM theophylline; anti-GPIbα, 50 μg ml^{-1} ALMA12 IgG. In all experiments, platelets were pretreated with MRS2179 (100 μM), 2-MeSAMP (10 μM) and indomethacin (10 μM) ($n = 3$ experiments). (**e**) DIC and epifluorescence imaging of the [Ca^{2+}] probe Oregon Green BAPTA-1 of a representative discoid platelet tethering to a platelet monolayer at an applied shear rate of 300 s^{-1}. Black arrows indicate a discoid platelet undergoing calcium spiking associated with tether restructuring; yellow arrowheads (332 and 397 s) indicate a discoid platelet undergoing transient filamentous tether formation in the absence of intracellular calcium flux. Scale bar, 2 μm. (**f**) Oregon Green BAPTA-1 fluorescence profile (arbitrary fluorescence units, AU) and concomitant discoid platelet tether length (μm) versus time for the representative platelet shown in **e**. Note that Oregon Green BAPTA-1 fluorescence increase correlates temporally with periods of tether shortening (representative of $n = 30$ experiments).

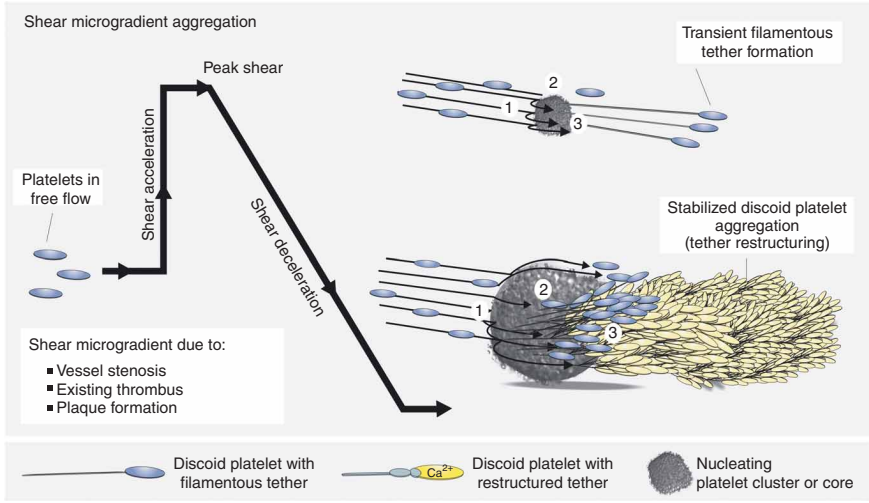

Figure 6 Working model of shear microgradient platelet aggregation. Blood flow perturbations caused by a partial luminal obstruction (a developing thrombus, an atherosclerotic plaque or an intravascular device), a change in vessel geometry (extrinsic constriction of blood vessels, vascular bifurcation or aneurysm) or sudden flow changes (vessel hypoperfusion due to shunting or upstream obstruction) can promote the development of shear microgradients. In combination with reactive thrombogenic surfaces, these shear microgradients can induce the formation of stabilized discoid platelet aggregates, the size of which is directly regulated by the magnitude and spatial distribution of the gradient. Shear microgradient–dependent platelet aggregation requires three principal features: shear acceleration phase, peak shear phase and shear deceleration phase. During shear acceleration phase, platelets in the bulk blood flow experiencing constant physiological shear are suddenly accelerated through the shear microgradient toward a peak shear threshold. During peak shear phase, a proportion of the discoid platelets that are accelerated into the peak shear zone adhere to exposed thrombogenic surfaces through GPIb. Exposure of these platelets to elevated hemodynamic drag forces leads to the extrusion of thin filamentous membrane tethers. Membrane tether formation initiates discoid platelet adhesion with the thrombogenic surface and also facilitates the recruitment of discoid platelets into the downstream deceleration zone. During shear deceleration phase, platelets transitioning into the flow deceleration zone experience decreasing hemodynamic drag forces. Reduced shear within this zone progressively favors the formation of integrin $\alpha_{IIb}\beta_3$ adhesion contacts. Integrin $\alpha_{IIb}\beta_3$ engagement is associated with low-frequency calcium spikes that trigger tether restructuring, leading to the stabilization of discoid platelet aggregates. Ongoing discoid platelet recruitment drives the propagation of the thrombus in the downstream deceleration zone, which may in turn amplify the shear microgradient and promote further platelet aggregation.

interactions beyond 8 s. In contrast, at a shear of 300 s^{-1}, 64 ± 14% of platelets showed overtly restructured tethers, resulting in an increase in cohesion lifetimes to a range of 8 s to >30 s (data not shown). This increase in adhesion lifetime was associated with adhesion strengthening, as discoid platelets with restructured tethers had a markedly increased ability to withstand the detaching effects of rapid shear increases (**Fig. 5c**). Approximately 75% of platelets with restructured tethers formed sustained adhesive interactions of >8-s duration after shear acceleration, compared to <10% of discoid platelets with thin filamentous tethers (**Fig. 5c**). These studies indicate that strengthening of discoid platelet cohesive interactions involves the physical restructuring of membrane tethers.

Mechanotransduction underlies tether restructuring

To gain insight into the underlying mechanisms regulating tether restructuring, we treated platelets with global inhibitors of platelet activation—prostaglandin E_1 (PGE_1) and the phosphodiesterase inhibitor theophylline (dimethylxanthine)—or with the actin polymerization inhibitor cytochalasin D. These inhibitors abolished tether restructuring and the associated adhesion strengthening, demonstrating that this phenomenon is activation dependent (**Fig. 5d**). Adhesion strengthening due to tether restructuring was calcium dependent, as it was abolished by chelation of extracellular Ca^{2+} (with EGTA) and by inhibition of inositol triphosphate-mediated calcium release (**Fig. 5d**). Furthermore, tether restructuring occurred independently of TXA_2, ADP and thrombin but required ligand binding to integrin $\alpha_{IIb}\beta_3$ (**Fig. 5d**). Imaging of Ca^{2+} flux showed that initial filamentous tether formation occurred without a detectable increase in Ca^{2+} concentration (**Fig. 5e**,**f**; 93 s); however, subsequent tether restructuring was associated with short duration Ca^{2+} spikes that correlated with phases of tether shortening or tensioning (**Fig. 5c**,**e**,**f**; 195 s; and **Supplementary Video 6** online). This transient Ca^{2+} flux was both IP_3 and extracellular Ca^{2+} dependent (data not shown) and occurred in the absence of global platelet shape change (**Fig. 5e**). These findings suggest that tether restructuring involves a localized Ca^{2+}-dependent signaling mechanism that occurs independently of global platelet activation.

To investigate the potential relevance of these calcium flux findings to stabilized discoid platelet aggregation *in vivo*, we analyzed the degree of platelet activation within discrete layers of forming thrombi by monitoring changes in cytosolic calcium flux ($\Delta[Ca^{2+}]_c$) and surface expression of the platelet α-granule protein, P-selectin (**Supplementary Fig. 6a–e** online). Discoid platelets undergoing transient tethering interactions with the surface of forming thrombi showed minimal $\Delta[Ca^{2+}]_c$ (**Supplementary Fig. 6a**) and had no detectable P-selectin expression (**Supplementary Fig. 6c**), whereas platelets within the stabilized discoid aggregate layers undergoing sustained adhesion showed transient $\Delta[Ca^{2+}]_c$ but minimal P-selectin levels, similar to those observed in platelets undergoing tether restructuring *in vitro* (**Supplementary Fig. 6a**,**d**). Platelets stably incorporated within the core of the thrombus showed sustained oscillatory $\Delta[Ca^{2+}]_c$ and measurable amounts of P-selectin, consistent with the role of soluble agonists in promoting full platelet activation in the thrombus base (**Supplementary Fig. 6a**,**e**). Taken together, these findings show that stabilized discoid platelet aggregation is associated with a low level of transient cytosolic flux that is sufficient to sustain platelet adhesive interactions independently of global platelet shape change and degranulation.

DISCUSSION

The studies presented here define a central role for shear microgradients in initiating the formation of stabilized discoid platelet aggregates during the early phases of thrombus development *in vivo*. This process is directly regulated by changes in blood hemodynamics and is crucial for the flow-directed propagation of thrombi downstream from the site of vessel injury. Although it has long been known that platelet aggregation typically occurs at sites of perturbed flow after vascular injury[19,20], it has been assumed that this process is directly caused by the accumulation of soluble platelet agonists at sites

of flow disturbance. Our studies challenge this hypothesis and suggest that platelets principally use a biomechanical platelet aggregation mechanism to promote the accumulation and stabilization of discoid platelets at sites of vascular injury.

Our studies show that local shear microgradients, which occur with changes in vessel geometry (stenosis) or as a consequence of thrombus formation itself, expose discoid platelets to rapidly changing hemodynamic conditions (specifically shear acceleration coupled to deceleration), leading to the development of stabilized discoid platelet aggregates (**Fig. 6**). Mechanistically, platelet exposure to sudden accelerations in shear promotes the development of membrane tethers, leading to the formation of transient discoid platelet aggregates[16]. We show that upon subsequent exposure to decelerating shear, these tethers physically restructure, increasing the strength and stability of discoid platelet aggregates, thereby promoting thrombus growth. This mechanosensitive adhesion mechanism occurs independently of soluble agonists and therefore represents a mechanism of stabilizing platelet adhesion at sites of vascular injury. Overall, our findings indicate that effective thrombus formation involves the cooperative interplay between two distinct, yet complementary, aggregation mechanisms, with stabilized discoid platelet aggregation representing the principal mechanism driving initial thrombus growth and soluble agonist generation primarily serving to stabilize formed aggregates.

Arterial thrombosis in the coronary or cerebrovascular circulations is the principal pathological process underlying the acute coronary syndromes and ischemic stroke, which together represent the leading cause of morbidity and mortality in industrialized societies. Despite recent improvements in antithrombotic therapies, the majority of patients receiving these drugs continue to die from acute thrombotic events[3,22]. Acute vascular occlusion represents the cumulative impact of atherosclerosis, superimposed thrombosis and vasoconstriction, with each of these processes having a major impact on vessel wall geometry and blood hemodynamics. Although the importance of perturbed hemodynamics in promoting thrombus formation has long been recognized[4,23–28], the molecular mechanisms underpinning these observations have remained ill defined. Our findings demonstrate that the magnitude and spatial distribution of shear microgradients correlate directly with the extent of platelet aggregation and that the resulting stabilized aggregates of discoid platelets have sufficient tensile strength to cause partial vascular occlusion, leading to a transient reduction in blood flow. The occlusive action of these aggregates, combined with their intrinsic instability and tendency to embolize to the distal circulation, raises the possibility that this aggregation mechanism may contribute to intermittent thromboembolic symptoms that are characteristic of the acute coronary syndromes and cerebrovascular disease. Furthermore, the demonstration that this aggregation process can occur independent of soluble agonists may help explain the limited antithrombotic efficacy of aspirin, clopidogrel and thrombin inhibitors, particularly in individuals with severe vascular disease[3].

Our findings help reconcile a number of fundamental controversies in the field, providing a mechanistic explanation for the observations that discoid platelets form aggregates *in vivo* independently of sustained calcium signaling[14,15] and that granule release and P-selectin expression on the surface of platelets occurs relatively late in the thrombotic process[17]. These findings also provide insight into the dynamic, heterogeneous adhesive behavior of platelets during initial thrombus growth[29]. In this context, a greater understanding of the fundamental relationship between alterations in blood rheology, membrane-tether restructuring and platelet aggregation may lead to the development of targeted antithrombotic therapies that are safer and more effective than existing approaches.

METHODS

Methods and any associated references are available in the online version of the paper at http://www.nature.com/naturemedicine/.

Note: Supplementary information is available on the Nature Medicine website.

ACKNOWLEDGMENTS

We thank Z. Ruggeri, H.H. Salem, R. Andrews and B. Kile for helpful feedback on the work; H. Blackburn and G. Rosengarten for advice and input on the CFD analysis; C. Nguyen for technical assistance in the analysis of *in vivo* blood flow rates; SciTech Proprietary Ltd. and Andor Proprietary Ltd. for the generous loan of a DV897CS EMCCD camera; M. Hickey (Monash University Department of Medicine, Monash, Australia) and A. Issekutz (Dalhousie University, Halifax, Canada) for providing the P-selectin–specific antibody; and C. Gachet (INSERM, Strasbourg, France) for *P2Y1*$^{-/-}$ mice. This work was supported by project funding from the National Health and Medical Research Council of Australia and the Australian Research Council. E.W. was supported by the National Heart Foundation of Australia.

AUTHOR CONTRIBUTIONS

W.S.N. designed the study and experiments, performed the *in vitro* platelet and micro-PIV experiments, codesigned vascular mimetics, performed microchannel perfusion experiments, analyzed data, supervised the study and cowrote the manuscript. E.W. designed experiments, performed the *in vivo* and *in vitro* experiments, analyzed data and assisted with manuscript preparation. F.J.T.-L. codesigned and fabricated vascular mimetics (microchannels), performed microchannel perfusion experiments and performed CFD simulations. E.T. performed and analyzed the micro-PIV experiments. J.F. performed *in vivo* experiments. A.M. codesigned the vascular mimetics and supervised their fabrication. J.C. supervised the micro-PIV analysis. A.F. designed and supervised the micro-PIV analysis and formulated and coded the micro-PIV analysis software. S.P.J. supervised the study and cowrote the manuscript.

Published online at http://www.nature.com/naturemedicine/
Reprints and permissions information is available online at http://npg.nature.com/reprintsandpermissions/

1. Trip, M.D., Cats, V.M., van Capelle, F.J. & Vreeken, J. Platelet hyperreactivity and prognosis in survivors of myocardial infarction. *N. Engl. J. Med.* **322**, 1549–1554 (1990).
2. Ruggeri, Z.M. Platelets in atherothrombosis. *Nat. Med.* **8**, 1227–1234 (2002).
3. Bhatt, D.L. & Topol, E.J. Scientific and therapeutic advances in antiplatelet therapy. *Nat. Rev. Drug Discov.* **2**, 15–28 (2003).
4. Virchow, R. Gesammelte abhandlungen zur wissenschaftlichen medicin. *Medsinger Sohn & Co.* 219–732 (1856).
5. Savage, B., Saldivar, E. & Ruggeri, Z.M. Initiation of platelet adhesion by arrest onto fibrinogen or translocation on von Willebrand factor. *Cell* **84**, 289–297 (1996).
6. Savage, B., Almus-Jacobs, F. & Ruggeri, Z.M. Specific synergy of multiple substrate-receptor interactions in platelet thrombus formation under flow. *Cell* **94**, 657–666 (1998).
7. Nesbitt, W.S. *et al.* Distinct glycoprotein Ib/V/IX and integrin $\alpha_{IIb}\beta_3$-dependent calcium signals cooperatively regulate platelet adhesion under flow. *J. Biol. Chem.* **277**, 2965–2972 (2002).
8. Nesbitt, W.S. *et al.* Intercellular calcium communication regulates platelet aggregation and thrombus growth. *J. Cell Biol.* **160**, 1151–1161 (2003).
9. Giuliano, S., Nesbitt, W.S., Rooney, M. & Jackson, S.P. Bidirectional integrin $\alpha_{IIb}\beta_3$ signalling regulating platelet adhesion under flow: contribution of protein kinase C. *Biochem. J.* **372**, 163–172 (2003).
10. Goncalves, I., Nesbitt, W.S., Yuan, Y. & Jackson, S.P. Importance of temporal flow gradients and integrin $\alpha_{IIb}\beta_3$ mechanotransduction for shear activation of platelets. *J. Biol. Chem.* **280**, 15430–15437 (2005).
11. Ruggeri, Z.M. & Mendolicchio, G.L. Adhesion mechanisms in platelet function. *Circ. Res.* **100**, 1673–1685 (2007).
12. Ruggeri, Z.M. The role of von Willebrand factor in thrombus formation. *Thromb. Res.* **120** Suppl 1, S5–S9 (2007).
13. Jackson, S.P. The growing complexity of platelet aggregation. *Blood* **109**, 5087–5095 (2007).
14. Dubois, C., Panicot-Dubois, L., Gainor, J.F., Furie, B.C. & Furie, B. Thrombin-initiated platelet activation *in vivo* is vWF independent during thrombus formation in a laser injury model. *J. Clin. Invest.* **117**, 953–960 (2007).
15. van Gestel, M.A. *et al.* Real-time detection of activation patterns in individual platelets during thromboembolism *in vivo*: differences between thrombus growth and embolus formation. *J. Vasc. Res.* **39**, 534–543 (2002).
16. Maxwell, M.J. *et al.* Identification of a 2-stage platelet aggregation process mediating shear-dependent thrombus formation. *Blood* **109**, 566–576 (2007).
17. Furie, B. & Furie, B.C. Thrombus formation *in vivo*. *J. Clin. Invest.* **115**, 3355–3362 (2005).

18. Ruggeri, Z.M., Orje, J.N., Habermann, R., Federici, A.B. & Reininger, A.J. Activation-independent platelet adhesion and aggregation under elevated shear stress. *Blood* **108**, 1903–1910 (2006).
19. Mustard, J.F., Jorgensen, L., Hovig, T., Glynn, M.F. & Rowsell, H.C. Role of platelets in thrombosis. *Thromb. Diath. Haemorrh. Suppl.* **21**, 131–158 (1966).
20. Mustard, J.F., Murphy, E.A., Rowsell, H.C. & Downie, H.G. Factors influencing thrombus formation in vivo. *Am. J. Med.* **33**, 621–647 (1962).
21. Dopheide, S.M., Maxwell, M.J. & Jackson, S.P. Shear-dependent tether formation during platelet translocation on von Willebrand factor. *Blood* **99**, 159–167 (2002).
22. Antithrombotic Trialists' Collaboration. Collaborative meta-analysis of randomised trials of antiplatelet therapy for prevention of death, myocardial infarction and stroke in high risk patients. *Br. Med. J.* **324**, 71–86 (2002).
23. Dintenfass, L. Rheologic approach to thrombosis and atherosclerosis. *Angiology* **15**, 333–343 (1964).
24. Stein, P.D. & Sabbah, H.N. Measured turbulence and its effect on thrombus formation. *Circ. Res.* **35**, 608–614 (1974).
25. Yoganathan, A.P., Corcoran, W.H., Harrison, E.C. & Carl, J.R. The Bjork-Shiley aortic prosthesis: flow characteristics, thrombus formation and tissue overgrowth. *Circulation* **58**, 70–76 (1978).
26. Schoephoerster, R.T., Oynes, F., Nunez, G., Kapadvanjwala, M. & Dewanjee, M.K. Effects of local geometry and fluid dynamics on regional platelet deposition on artificial surfaces. *Arterioscler. Thromb.* **13**, 1806–1813 (1993).
27. Eckstein, E.C., Tilles, A.W. & Millero, F.J. III. Conditions for the occurrence of large near-wall excesses of small particles during blood flow. *Microvasc. Res.* **36**, 31–39 (1988).
28. Wang, S.K. & Hwang, N.H. On transport of suspended particulates in tube flow. *Biorheology* **29**, 353–377 (1992).
29. Kulkarni, S. *et al.* A revised model of platelet aggregation. *J. Clin. Invest.* **105**, 783–791 (2000).

ONLINE METHODS

Materials. Lepirudin was from Pharmion; apyrase, hexamethyldisilazane (HMDS), MRS2179, 2-MesAMP, indomethacin, EGTA, cytochalasin D (CD), theophylline, 2-aminoethoxydiphenylborate (2-APB) and PGE_1 were from Sigma; Rose Bengal was from Acros Organics; c7E3 Fab was from Eli Lilly; Oregon Green BAPTA-1 was from Molecular Probes; ALMA12 antibody was provided by F. Lanza (Institut National de la Santé et de la Recherche Médicale (INSERM) U.311, Strasbourg, France); and RMP-$1^{Alexa488}$ was provided by A. Issekutz (Dalhousie University, Halifax, Canada).

Platelet preparation. Washed platelets were isolated from anticoagulated whole blood taken from consenting human donors according to a previously described method[30]. Lepirudin (1 U ml^{-1}) was included in platelet washing buffer (4.3 mM K_2HPO_4, 4.3 mM Na_2HPO_4, 24.3 mM NaH_2PO_4, 113 mM NaCl, 5.5 mM D-glucose and 10 mM theophylline, pH 6.5, with 0.02 U ml^{-1} apyrase) in Tyrode's buffer (10 mM HEPES, 12 mM $NaHCO_3$, 137 mM NaCl, 2.7 mM KCl and 5 mM glucose, pH 7.3). We obtained approval for these studies from the Monash University Standing Committee on Ethics in Research Involving Humans.

Intravital studies. Approval was obtained from the Alfred Medical Research and Education Precinct Animal Ethics Committee for all experiments involving animals. We performed intravital studies according to a modification of a previously published method[31,32]. We used C57BL/6 wild-type mice weighing 18–20 g (Alfred Medical Research and Education Precinct Animal Services (AMREP AS Pty Ltd)), and *P2Y1*$^{-/-}$ mice (previously described[33,34]). We anesthetized mice (60 mg per kg body weight sodium pentabarbitone) and injured their mesenteric arterioles (60–160 μm) via photoactivation (excitation at 550 nm, 10–30 s) of systemically administered Rose Bengal (5 mg per kg body weight)[35], microinjection of 6% $FeCl_3$ into the tissue adjacent to the arteriole of interest[36], mechanical puncture of the vessel wall with a microinjector needle (tip diameter 4–6 μm) or mild crush injury induced by ligation of the vessel with a blunted microinjector needle (tip diameter 30–60 μm). For the *in vivo* stenosis experiments, we administered *P2Y1*$^{-/-}$ mice, at time points of –24 h and –2 h, 200 mg per kg body weight aspirin and either 10 mg per kg body weight clopidogrel (causing an ~50% reduction in ADP-induced platelet aggregation) or 50 mg per kg body weight clopidogrel orally (causing complete inhibition of ADP-induced platelet aggregation). In studies using hirudin, we intravenously infused mice with high-dose hirudin (50 mg per kg body weight) 5 min before the onset of vascular injury. In control studies, we confirmed the effectiveness of each of these antagonists by performing *ex vivo* platelet functional assays or through coagulation testing[37,38]. We monitored P-selectin expression after $FeCl_3$-induced thrombus formation in the presence of systemically administered P-selectin–specific antibody coupled to Alexa488 fluorophore (RMP-$1^{Alexa488}$, obtained from M. Hickey; 1.3 mg per kg body weight) and recorded with an ANDOR DV897DCS electron-multiplying charge-coupled device (EM-CCD). We visualized platelet interactions by DIC microscopy using a Leica DMIRB inverted microscope (objectives: 100× PL APO, numerical aperture 1.40–0.7 and 63× HCX PL APO, numerical aperture 1.2) and a DAGE MTI charge-coupled device camera.

Microchannel fabrication. We fabricated microchannels in polydimethylsiloxane (Sylgard) from a KMPR 1025 (polymethylglutarimide) photoresist (MicroChem) mold on a 3-inch silicon wafer according to a modification of a published method[39]. We used a high-resolution chrome mask to attain well defined features to construct the mold. The overall channel depth was 80 μm.

Flow studies and analysis of tether restructuring. We performed flow assays according to a modification of a published method[32]. We derivatized dried microcapillaries with hexamethyldisilazane for 15 min at 21 °C and washed them with double-distilled water. For monolayer experiments, we allowed platelets in Tyrode's buffer (6×10^8 per ml) supplemented with 2 mM EGTA to spread for 15 min, and then incubated them with BSA (20 mg ml^{-1}) for 5 min. We preincubated washed platelets for 10 min with MRS2179 (100 μM), 2-MesAMP (10 μM) and indomethacin (10 μM) in Tyrode's buffer supplemented with 1 mM Ca^{2+} before reconstitution with washed red blood cells (50% vol/vol) (containing 0.02 U ml^{-1} apyrase and 1 U ml^{-1} lepirudin). Before reconstitution, we preincubated washed platelets with either of the following inhibitors: EGTA (5 mM), c7E3 Fab (30 μg ml^{-1}), cytochalasin D (20 μM), 2-aminoethoxydiphenylborate (2-APB) (50 μM), ALMA12 (50 μg ml^{-1}) or combined PGE_1 (10 μg ml^{-1}) and theophylline (10 mM). We performed perfusion studies at wall shear rates of 300 s^{-1} (monolayer experiments). We visualized adherent platelets by DIC microscopy (100× PL APO objective, numerical aperture 1.40–0.7) on a Leica DMIRB microscope. We monitored adhesion over a 300-s period and video-recorded it for offline analysis. Thirty seconds after the start of the flow, we analyzed the tethering time of platelets (cohesion lifetime) frame by frame (25 frames per second). We set the maximum cohesion lifetime cutoff to 30 s. We included only platelets with a discoid morphology in the analysis.

Microparticle image velocimetry. We conducted micro-PIV experiments according to a modification of a published method[40,41] (**Supplementary Methods** online).

Bead collision assay. We performed bead collision assays according to a modification of a published method[42] (**Supplementary Methods**).

Analysis of platelet calcium flux. We monitored platelet calcium flux, with minor modifications, as previously described[43] (**Supplementary Methods**).

Computational fluid dynamics. We calculated estimates of shear rates after solving the velocity field using the conservation of mass and momentum equations for an incompressible fluid flow, using the CFD software package FLUENT 6.0 (Fluent USA) based on a finite volume scheme[44]. We assumed the validity of the continuum hypothesis and no-slip boundary condition. We considered the flow to be three-dimensional, steady, laminar and incompressible. We considered the fluid medium to have a constant density of 998.2 km m^{-3} and viscosity of 0.00345 Pa s. Discretization scheme pressure was set as standard, and the second-order upwind momentum option was enabled. For the case where vessel stenosis was localized to the site of vessel injury (**Fig. 1a**), we modeled the geometry of the blood vessel with SolidWorks v. 2004 (SolidWorks Corp.) using a blood vessel diameter of 42 μm and an idealized geometry derived from video footage of the *in vivo* stenosis (**Fig. 1a**). No elastic effects were considered, keeping the perimeter of the transversal section of the blood vessel constant. We transferred the geometry into a specialized preprocessing grid generation (Fluent, Gambit) to generate a structured mesh of 76,800 elements. For modeling bead collision in microchannels, the mesh consisted of two zones, an unstructured region close to the bead and a structured mesh everywhere else. We applied a symmetry condition at the center plane of the beads. The number of cells in the structured mesh generated was directly dependent on bead size ranging from 754,446 (2-μm beads) to 954,516 (15-μm beads).

Statistical analyses. Results are presented as mean ± s.e.m. for bar graphs and median for dot plots. We assessed statistical significance by Student's *t*-test. We drew schematics with CorelDraw Graphics Suite (Corel). We digitized video using Pinnacle Systems DV500 PLUS (Pinnacle Systems) and edited it with Adobe Premiere Pro v1.5 (Adobe Systems).

30. Schoenwaelder, S.M. *et al.* Identification of a unique co-operative phosphoinositide 3-kinase signaling mechanism regulating integrin α3 adhesive function in platelets. *J. Biol. Chem.* **282**, 28648–28658 (2007).
31. Denis, C. *et al.* A mouse model of severe von Willebrand disease: defects in hemostasis and thrombosis. *Proc. Natl. Acad. Sci. USA* **95**, 9524–9529 (1998).
32. Kulkarni, S. *et al.* Techniques to examine platelet adhesive interactions under flow. *Methods Mol. Biol.* **272**, 165–186 (2004).
33. Léon, C. *et al.* Defective platelet aggregation and increased resistance to thrombosis in purinergic P2Y(1) receptor-null mice. *J. Clin. Invest.* **104**, 1731–1737 (1999).
34. Mayadas, T.N., Johnson, R.C., Rayburn, H., Hynes, R.O. & Wagner, D.D. Leukocyte rolling and extravasation are severely compromised in P selectin-deficient mice. *Cell* **74**, 541–554 (1993).
35. Rosen, E.D. *et al.* Laser-induced noninvasive vascular injury models in mice generate platelet- and coagulation-dependent thrombi. *Am. J. Pathol.* **158**, 1613–1622 (2001).
36. Kurz, K.D., Main, B.W. & Sandusky, G.E. Rat model of arterial thrombosis induced by ferric chloride. *Thromb. Res.* **60**, 269–280 (1990).
37. Sturgeon, S.A., Jones, C., Angus, J.A. & Wright, C.E. Advantages of a selective β-isoform phosphoinositide 3-kinase antagonist, an anti-thrombotic agent devoid of other cardiovascular actions in the rat. *Eur. J. Pharmacol.* **587**, 209–215 (2008).
38. Mangin, P. *et al.* Thrombin overcomes the thrombosis defect associated with platelet GPVI/FcRgamma deficiency. *Blood* **107**, 4346–4353 (2006).

39. Weibel, D.B., Diluzio, W.R. & Whitesides, G.M. Microfabrication meets microbiology. *Nat. Rev. Microbiol.* **5**, 209–218 (2007).
40. Fouras, A., Lo Jacono, D. & Hourigan, K. Target-free stereo PIV: a novel technique with inherent error estimation and improved accuracy. *Exp. Fluids* **44**, 317–329 (2008).
41. Fouras, A.S.J. Accuaracy of out-of-plane vorticity measurements derived from in-plane velocity field data. *Exp. Fluids* **25**, 409–430 (1998).
42. Edmondson, K.E., Denney, W.S. & Diamond, S.L. Neutrophil-bead collision assay: pharmacologically induced changes in membrane mechanics regulate the PSGL-1/P-selectin adhesion lifetime. *Biophys. J.* **89**, 3603–3614 (2005).
43. Yap, C.L. *et al.* Synergistic adhesive interactions and signaling mechanisms operating between platelet glycoprotein Ib/IX and integrin alpha IIbbeta 3. Studies in human platelets and transfected Chinese hamster ovary cells. *J. Biol. Chem.* **275**, 41377–41388 (2000).
44. Versteeg, H. & Malalasekrera, W. *An Introduction to Computational Fluid Dynamics: The Finite Volume Method* (Longman Scientific & Technical, Harlow, UK, 1995).

doi:10.1038/nm.1955